ELSEVIER

Journal of Nuclear Materials 295 (2001) 31–41

journal of nuclear materials

www.elsevier.nl/locate/jnucmat

Effect of Mo addition on the crystal texture and deformation twin formation in Zr-based alloys

Y.B. Chun [a], S.K. Hwang [a,b,*], M.H. Kim [a], S.I. Kwun [c], S.W. Chae [d]

[a] *Department of Metallurgical Engineering, Inha University, Incheon 402-751, South Korea*
[b] *Center for the Advanced Aerospace Materials, South Korea*
[c] *Department of Materials Science and Engineering, Korea University, Seoul 136-701, South Korea*
[d] *Department of Mechanical Engineering, Korea University, Seoul 136-701, South Korea*

Received 4 July 2000; accepted 6 February 2001

Abstract

The effect of Mo on the crystal texture of Zr–Nb and Zr–Nb–Mo alloys was studied. Molybdenum addition reduced the average sizes of the equiaxed α grains and the packets considerably. In the Zr–Nb alloy specimens free of Mo, the intensity of the normal basal texture increased with the initial grain size, which was attributed to the enhanced probability of twinning in coarse grains. Molybdenum also reduced the intensity of the normal basal texture of the Zr alloys, indicating a possible change in the mode of deformation caused by Mo addition. Moreover, the texture shift of the Zr alloys from ND–TD to ND–RD during annealing heat treatment was accelerated by Mo addition. Weakening of the normal basal texture in the cold-worked Mo-containing alloy, therefore, was attributed to the microstructural refinement and the change in the deformation mode.

PACS: 81.05.Bx; 61.72.Mm; 81.40.Ef

1. Introduction

Zr-based alloys are widely used as core materials for nuclear reactors. Being a HCP crystal structure, the Zr-based alloys retain a high intensity of crystal textures created by deformation and heat treatment during production into either tubular or plate shape. The crystal texture has a large influence on the anisotropic mechanical strength, radiation-induced growth, creep and stress-induced delayed hydride cracking of the alloys [1–4]. For the case of pressure tubes in heavy water reactors, a strong radial basal texture is preferred for improving the resistance to delayed hydride cracking whereas a tangential basal texture is more favorable under irradiation-induced growth and creep circumstances. For the case of fuel cladding in light water reactors a radial basal texture is desirable for the anisotropic strength and the resistance to iodine stress corrosion cracking. Therefore control of texture is important in optimizing the performance of the Zr-based alloys.

In an earlier study, we reported a beneficial effect of Mo addition on the yield strength of Zr–Nb and Zr–Nb–Sn alloys. This effect was attributed to solid solution hardening and retardation of grain growth during recrystallization annealing treatment, which resulted in a remarkably fine microstructure [5–7]. These effects of Mo were accompanied by a substantial change in crystal texture. Thin plate Zr-alloy samples in general showed a reduced normal basal texture with Mo addition [6]. Crystal texture in Zr-alloys is known to be sensitive to materials processing parameters, particularly during plastic deformation [8–10]. Deformation twins, for example, are cited for the prime reason for texture formation. Due to the lack of the independent slip systems, twinning accommodates plastic strain in Zr-alloys [11]. Since twinning involves lattice rotation it is surmised that the crystal texture is closely related to the twinning propensity [12]. There is a lack of study, however, that

* Corresponding author. Tel.: +82-32 860 7537; fax: +82-32 862 5546.
E-mail address: skhwang@inha.ac.kr (S.K. Hwang).

0022-3115/01/$ - see front matter
PII: S0022-3115(01)00490-1

correlates the effect of alloying elements, Mo in particular, with the crystal texture in terms of twinning. The present work was aimed to find the relationship between the change in microstructure and twinning tendency caused by Mo addition in Zr–Nb alloys so as to explain the effect of Mo on crystal texture.

2. Experimental procedure

Experimental materials of four different alloy compositions were prepared: Zr–1Nb, Zr–1Mo, Zr–1Nb–0.7Mo and Zr–2.5Nb. The first three compositions were experimentally designed compositions to study the effect of Mo with or without Nb co-present, and the last composition is that of the commercial alloy used for the heavy water reactor. Nuclear grade sponge Zr and pellet-shape Mo and Nb in 99.95% and 99.9% purity, respectively, were used for the alloy preparation. These elements were alloyed by plasma arc re-melting (four times) and cast into buttons of 300 g in weight. The chemical compositions of the experimental alloys are shown in Table 1. Buttons were forged at 1100°C by 40% in thickness and β-annealed at 1000°C for 30 min, and then water-cooled. Prior to cold rolling, another annealing heat treatment was conducted to improve the workability: 1000°C for 10 min and then furnace-cooled. Compression testing was conducted at room temperature. Test specimens were shaped into 6 mm × 6 mm × 9 mm square pillar and gage length was 9 mm, height of square pillar. A crosshead speed of 1 mm/min was maintained during test.

For the analysis of the crystal texture, an X-ray diffractometer attached with a goniometer was used. Diffraction was made by Mo–K_α beam activated under 40 kV and 30 mA. Schulz reflection method was used to obtain (0 0 0 2) direct pole figures within the range of 0–70° by measuring the diffracted beam intensity at an interval of 5°. The direct pole figures were standardized using randomly oriented Zr powder sample. Inverse pole figures were also obtained, from which the Kearns number f was calculated [13]. Since the specimens for this analysis were prepared from the cold-rolled plate the Kearns number in this paper refers to the intensity of the basal poles aligned to the surface normal direction, i.e., f_n.

The etching solution used for the optical microscopy consisted of hydrofluoric acid, nitric acid and water in the volume ratio of 5:45:50 whereas the electro-thinning solution for the transmission electron microscopy (TEM) consisted of hydrochloric acid and methanol in the volume ratio of 1:9. Electro-thinning was conducted at −40°C under the condition of 5 V and 20 mA.

Table 1
Chemical compositions of experimental alloys

Nominal	Analysis (wt%)		
	Nb	Mo	Zr[a]
Zr–1Mo	–	1.10	Bal.
Zr–2.5Nb	2.60	–	
Zr–1Nb	1.01	–	
Zr–1Nb–0.7Mo	1.02	0.75	

[a] The nuclear grade sponge Zr used in present study contained 38 ppm carbon, 533 ppm oxygen, 422 ppm Fe, 44 ppm Hf and 10 ppm Si prior to melting. During melting and subsequent treatment, the residual oxygen content of these alloys increased to approximately 1000 ppm.

3. Results and discussion

3.1. Effect of cold reduction on texture

The Kearns numbers of cold-rolled experimental alloys were obtained. For the case of Zr–1Nb alloy, the Kearns numbers were obtained as a function of the amount of cold work varying from 10% to 82% and the result is shown in Table 2 and Fig. 1.

In the β-annealed condition, the alloy showed a random texture, as indicated by the f_n value close to 0.33. The intensity of the normal basal texture rapidly increased with cold work, reaching to $f_n = 0.73$ at 65% of cold work. A saturation of the texture intensity occurred at about 82% of cold work, at which point the f_n value was about 0.76. The abrupt increase of the texture during the initial phase of cold work and the saturation of the texture intensity at a large amount of cold work is a general phenomenon in Zr-based alloys reported in literatures [14].

Variation of the texture intensity as a function of the amount of cold work can be explained in terms of the mechanism of plastic deformation. In the beginning of deformation when the deformation is small (0–50%), twinning primarily governs the texture formation [6,12,14]. Twinning causes an extensive rotation of

Table 2
Variation of the normal basal texture, f_n, of as cold-rolled Zr–1Nb alloy as a function of the amount of cold work and the through-thickness depth of specimen plates

Materials condition	f_n				
	Surface	75%	50%	25%	Center
As β-annealed	0.32	0.35	0.34	0.31	0.34
As 10% cold-rolled	0.44	0.44	0.45	0.46	0.46
As 30% cold-rolled	0.58	0.65	0.66	0.63	0.62
As 50% cold-rolled	0.68	0.69	0.70	0.68	0.69
As 65% cold-rolled	0.67	0.74	0.73	0.73	0.73
As 70% cold-rolled	0.68	0.75	0.76	0.75	0.75
As 78% cold-rolled	0.68	0.76	0.75	0.75	0.76
As 82% cold-rolled	0.70	0.76	0.76	0.77	0.76

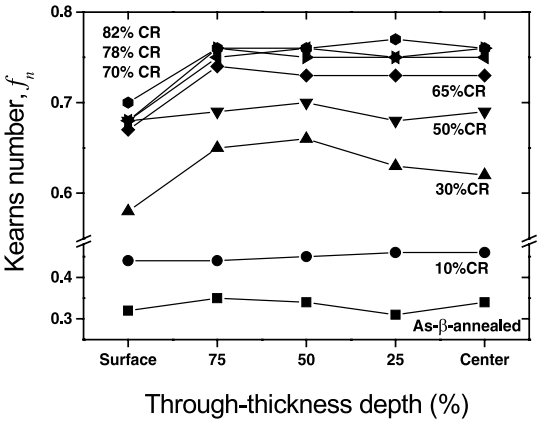

Fig. 1. Variation of the surface normal basal texture as a function of the amount of deformation and of the through-thickness depth of cold-rolled Zr–1Nb alloy. Note the uneven through-thickness distribution of the texture intensity at an intermediate level of cold work.

crystal lattice in such a way that further deformation is resisted, resulting in a strong texture formation. With increased deformation, however, the mode of deformation shifts from twinning to slip. There are two reasons why this occurs: first, exhaustion of grains favorably oriented for twinning and secondly a grain refinement due to twinning [15]. The grain refinement occurs because twinning essentially produces new boundaries due to substantial difference in crystal orientation with those of neighboring grains. Grain refinement, in turn, restricts further twinning.

It is noted in Table 2 that the texture intensity varied with the thickness of specimens. Kearns number showed about 10% difference between the middle and the near-surface region of specimens. A similar phenomenon was also reported in tube-type Zr-based alloys [16]. The gradient in the texture intensity in the present case was probably caused by the difference in the amount and the mode of plastic deformation during rolling of plate-type specimens [17]. Interestingly, the uneven distribution of the texture intensity was most severe in the specimen cold-rolled by about 30%. In the as β-annealed specimens and heavily cold-worked specimens, the texture was homogeneous throughout most thickness.

3.2. Effect of alloying elements on texture

The microstructures of as β-annealed Zr–1Nb and Zr–1Nb–0.7Mo alloys are shown in Fig. 2. Elongated α-platelets formed packets that filled the entire space. Each platelet shows a crystallographic feature of directional growth, which originated from Widmanstätten-type transformation route of α-phase from the high temperature β-phase upon cooling [18]. Although this micro-

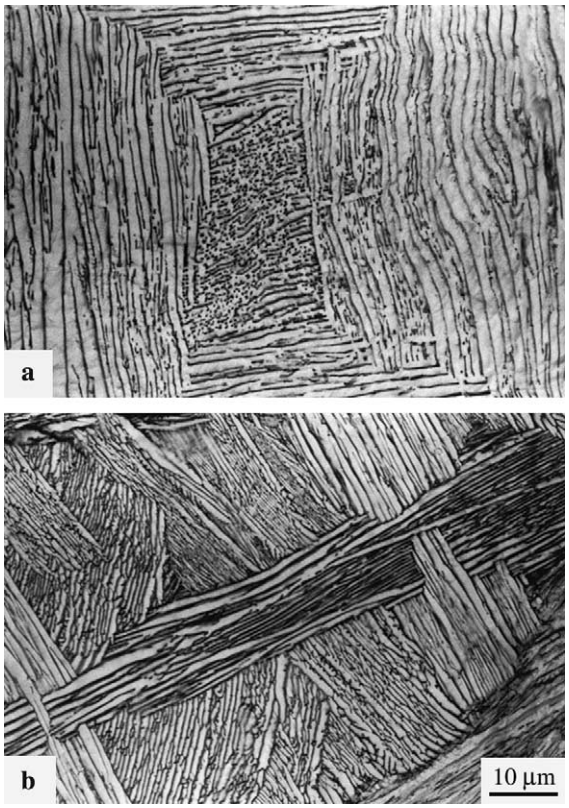

Fig. 2. Optical micrographs of (a) Zr–1Nb and (b) Zr–1Nb–0.7Mo alloys all in β-annealed condition. Widmanstätten-type α-platelets, which originated from the high-temperature β-phase, form packets. The widths of the platelets as well as the average size of packets decreased with Mo addition.

structural characteristic was consistently observed in all experimental alloys, the width of α-platelets varied with the chemical composition. For example, the widths of α-platelets in Zr–1Nb and Zr–1Nb–0.7Mo were 1–2 μm and less than 1 μm, respectively. The average size of the packets of α-platelets showed a similar trend: 50–200 μm in Zr–1Nb vs. 10–50 μm in Zr–1Nb–0.7Mo. Therefore the previous report [6,7] of the present authors on the grain-refining effect of Mo in Zr-based alloys was confirmed. Existence of Mo in β-phase probably retarded the growth of α-platelets by lowering the mobility of the α/β interface.

Since the texture variation with the amount of cold work saturated at heavy deformation, the texture intensities of the experimental alloys were compared at a fixed amount of thickness reduction, 70%, and the result is shown in Table 3. The heavy cold work remarkably intensified the normal basal texture of all the alloys. Among the alloys of different composition, Nb-containing alloys resulted in greater texture intensification than the Mo-containing alloys. Because of the lack of

Table 3
Variation of the normal basal texture, f_n, of the experimental Zr-based alloys in β-annealed condition and heavily cold-worked condition

	As β-annealed		70% cold-rolled	
	α-platelet width (μm)[a]	f_n	α-platelet width (μm)	f_n
Zr–1Mo	1.1±0.03	0.31	0.9	0.63
Zr–2.5Nb	1.7±0.07	0.36	1.0	0.65
Zr–1Nb	2.2±0.16	0.36	1.6	0.68
Zr–1Nb–0.7Mo	1.0±0.08	0.33	0.8	0.61

[a] The scatter image in the data denotes the standard error of measurements.

data on systematic variation of the chemical composition and their corresponding texture properties, however, the quantitative effect of the alloy composition on texture is inconclusive. Nevertheless, irrespective of the alloy composition, a consistent effect of the microstructural parameter on texture could be discerned as shown in Fig. 3. In this figure, the width of α-platelets in β-annealed state is regarded as the microstructural parameter substituting the grain size since the grain size of the experimental alloys in the cold-rolled condition was difficult to measure.

When the experimental Zr-based alloys were deformed by compression, deformation twins appeared on the surface of test specimens, examples of which are shown in Fig. 4. The twins appeared at a compression strain as low as 8%. Two characteristic features of the twins were observed: first, twins were inclined to the axis of compression within 30–60° and secondly, twins were also inclined, not parallel, to the axis of the α-platelet.

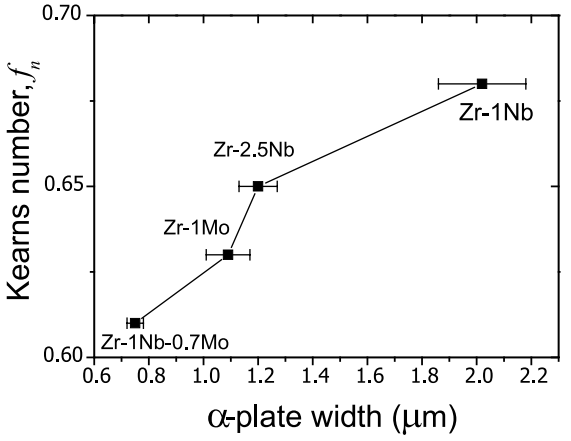

Fig. 3. Variation of the normal basal texture of the experimental Zr-based alloys in 70% cold-rolled condition as a function of the width of the α-platelets in β-annealed state prior to cold rolling. Note the effect of the α-platelet width on increasing the texture intensity irrespective of the chemical composition of the alloys.

An effect of alloying element was observed on twin formation. In case of Zr–1Nb alloy, the length and the width of twin plates ranged 20–200 μm and 5–10 μm, respectively. Molybdenum addition in the Zr–1Nb alloy reduced the frequency of twins as well as the length of individual twin plates although it did not affect the width of twins. The length of twins in Zr–1Nb–0.7Mo alloy was in the range of 20–50 μm.

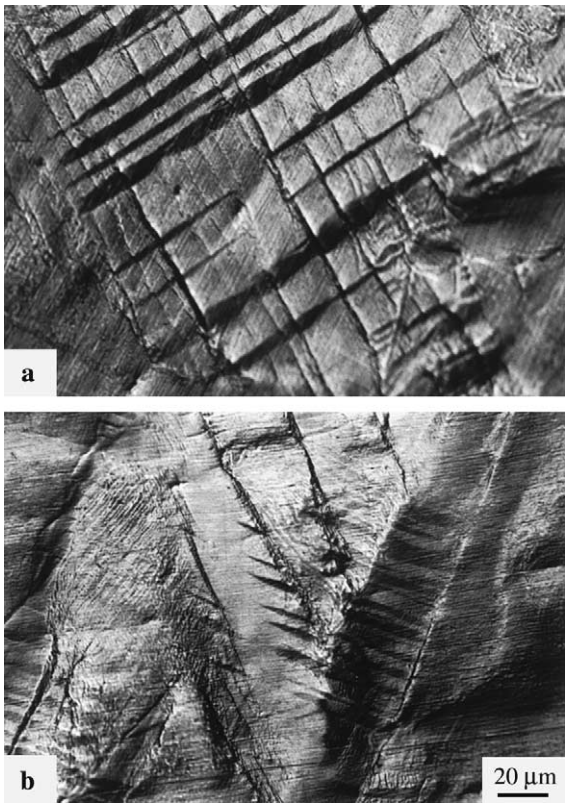

Fig. 4. Optical micrographs of the surface of (a) Zr–1Nb and (b) Zr–1Nb–0.7Mo alloy specimens compressed by 8% showing deformation twins on the specimen surfaces polished prior to deformation test. The frequency of twins and the length of twin plates decreased with Mo addition.

The effect of Mo on deformation twins was correlated with the microstructure prior to compression loading. Twins formed within a packet of α-platelets in the bulk of Zr–1Nb–0.7Mo alloy are shown in Fig. 5. The twin plates crossed α-platelets but the growth of the twins stopped at a packet boundary. It was pointed out above that Mo reduced the packet size of Zr–1Nb alloy. Therefore it was concluded that the effect of Mo on reducing the twin frequency and the length of twin plates was a consequence of reduced α-platelet packet size. This conclusion was further supported by the fact that the average size of the α-platelet packets coincided with the maximum size of twin plates after compression deformation.

It is conceivable that growth characteristics of deformation twins across α-platelet boundaries in Zr–1Nb alloy may also be affected by Mo addition. In the previous work [6,7] the present authors reported that the boundaries of α-platelets were enriched with β-stabilizing elements such as Nb and Mo. As a result, a thin layer of β-phase frequently formed at the α-platelet boundaries, which was expected to hinder the growth of twins. The twins that were blocked halfway across the packet boundary, as shown in Fig. 4(b), probably encountered many obstacles of the thin inter-platelet β-phases in their wake.

Appearance of twins indicates the twinning system, from which the effect of alloying addition on twinning system can be deduced. For example, twins corresponding to a large shear, such as $\{1\,1\,\bar{2}\,1\}\langle 1\,1\,\bar{2}\,\bar{6}\rangle$ ($s = 0.63$, s: shear strain) are thinner than those of small shear, such as $\{1\,0\,\bar{1}\,1\}\langle\bar{1}\,0\,1\,2\rangle 1$ ($s = 0.10$). The extent of deformation may also influence the thickness of twins [19]. In the present result, the thickness of twins formed under a constant strain of 8% did not vary with Mo addition. Therefore it may be concluded that the effect of Mo on the twinning system of Zr–1Nb, if any, was negligible. It will be shown, however, that Mo addition does affect the tendency of twinning.

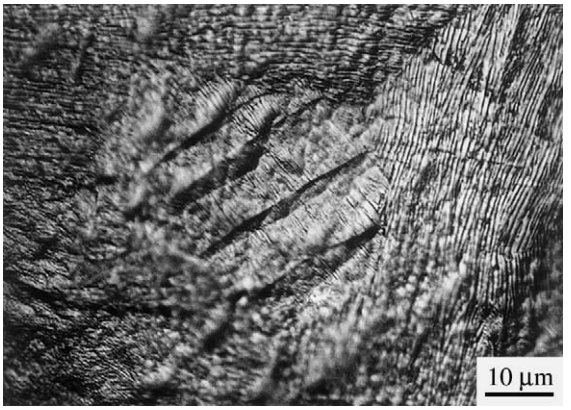

Fig. 5. Optical micrograph of twins in Zr–1Nb–0.7Mo alloy compression deformed by 8%, showing the growth of twins blocked by the boundaries of α-platelet packets. The specimen surface was pre-etched prior to deformation and photographing.

With substantially increased deformation, the effect of Mo on twinning became obliterated. The specimens of Zr–1Nb and Zr–1Nb–0.7Mo that were compression deformed by 18% revealed extensive amount of twins as shown in Fig. 6. Deformation twins produced on different variants of twinning systems crossed each other. A high density of twins was found in both alloys without a clear difference in twin density between the two. In addition, the surface relief caused by high deformation also made it difficult to discern the effect of Mo addition on twinning.

In order to interpret the effect of alloying elements on crystal texture, it is essential to know their effect on grain size. The grain size variations of all the experimental alloys as a function of annealing time at 800°C

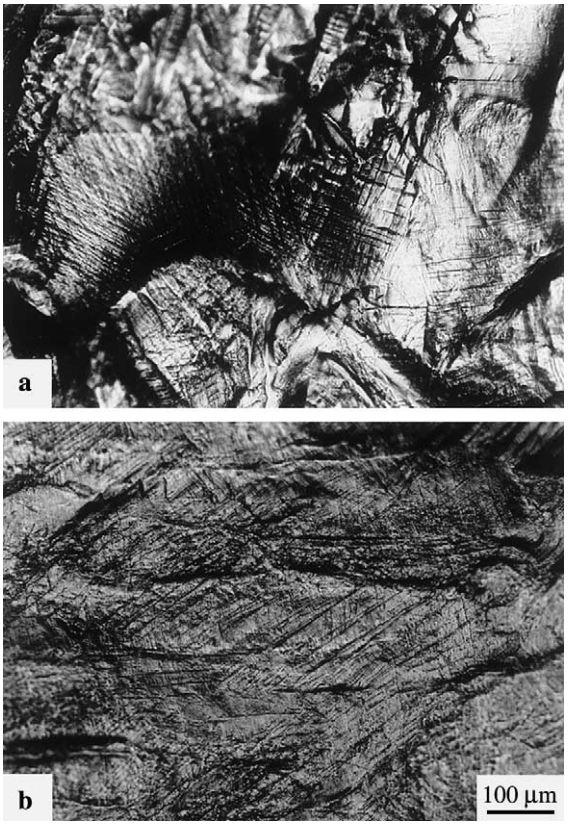

Fig. 6. Optical micrographs of the surface of (a) Zr–1Nb and (b) Zr–1Nb–0.7Mo alloy specimens compressed by 18% showing a high density of deformation twins. In contrast to the small deformation case shown in Fig. 4, the effect of Mo is not clearly discernible due to the high density of twins and extensive surface relief.

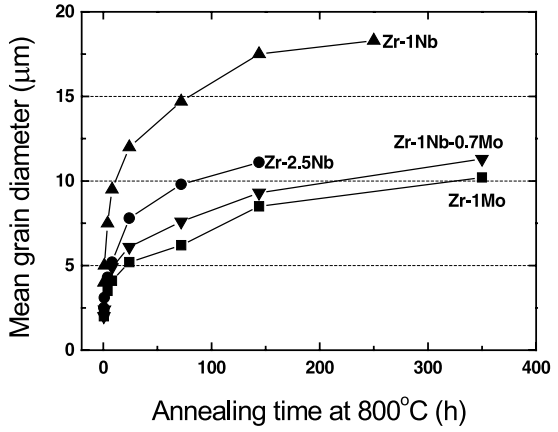

Fig. 7. Grain growth characteristics of experimental Zr-based alloys during annealing heat treatment at 800°C. Increasing the concentration of the alloying elements retarded the rate of grain coarsening and the equilibrium grain size, Mo being of the greatest effect.

are shown in Fig. 7. All the alloys showed recrystallization and subsequent grain coarsening to equiaxed grains after the heat treatment. Among the four alloys, Zr– 1Nb showed the largest equilibrium grain size whereas Zr–1Mo showed the smallest grain size, about half of that of Zr–1Nb. The equilibrium grain size was proportional to the average grain size established in the early stage of recrystallization. Increasing Nb content from 1% to 2.5% reduced the grain size; however, this effect was smaller compared to that of adding 1% Mo to Zr or 0.7% Mo to Zr–1Nb. Addition of 0.7Mo to Zr–1Nb alloy retarded the grain coarsening almost to

Table 4
Variation of the normal basal texture, f_n, of the experimental Zr-based alloys in annealed condition and subsequently cold-rolled condition

	As annealed at 800°C			55% cold-rolled
	Annealing time (h)	Grain size (μm)	f_n	f_n
Zr–1Mo	0.5	2.0	0.55	0.62
	20	5.2	0.56	0.64
	350	10.2	0.56	0.63
Zr–2.5Nb	0.5	2.5	0.61	0.61
	8	5.1	0.57	0.65
	75	9.9	0.56	0.70
Zr–1Nb	0.5	4.0	0.59	0.60
	1	5.5	0.59	0.61
	20	10.1	0.61	0.63
	250	18.3	0.6	0.66
Zr–1Nb–0.7Mo	0.5	2.0	0.57	0.61
	8	4.1	0.55	0.62
	75	9.0	0.57	0.60
	350	11.3	0.54	0.61

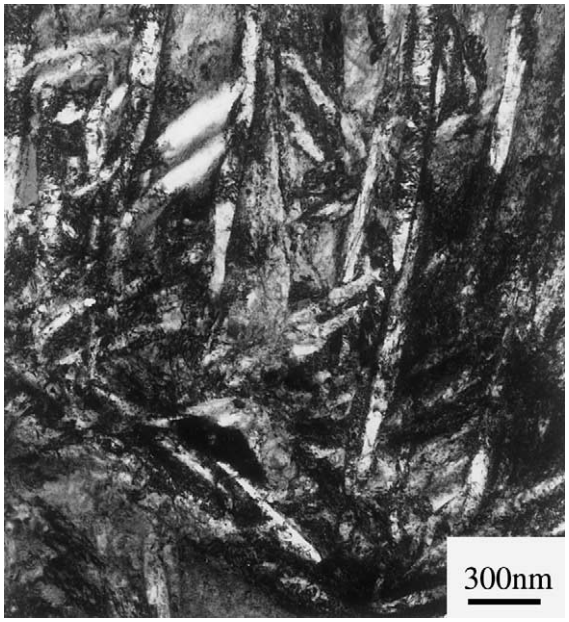

Fig. 8. TEM image of β-phase formed in Zr–1Nb–0.7Mo exposed to 800°C for 350 h and subsequently cooled to the ambient temperature. Various habit planes of the transformed plates are a result of the Burger's orientation relationship between β and α phases, which resulted in a reduction of the normal basal texture.

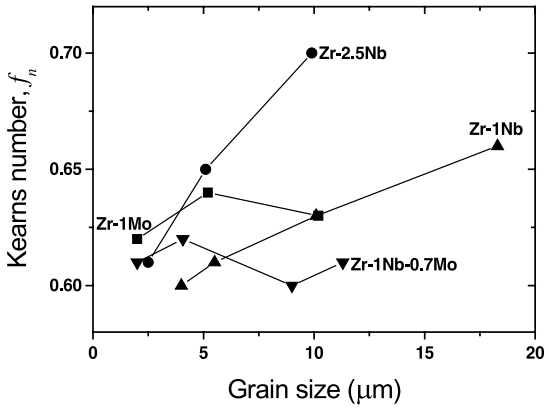

Fig. 9. Relationship between the size of equiaxed grains formed during recrystallization and the normal basal texture of Zr-based experimental alloys. While Zr–Nb alloys showed a proportional relationship between the two parameters the Mo-containing alloys showed constant texture intensity irrespective of the grain size.

the level of Zr–1Mo. As pointed out above, β-phases forming at the boundaries of α-platelets seemed to resist coarsening of microstructure through coalescence of the platelets [20]. In the same context, the inter-platelet β-phase also resisted abnormal grain coarsening in Zr–Nb alloys. Therefore it may be concluded that Mo addition increased the volume fraction as well as the stability of the inter-platelet β-phase, thereby resulted in grain refinement and suppressed abnormal grain growth.

3.3. Effect of grain size on texture

Upon exposure to an α-annealing temperature of 800°C and subsequent cooling to ambient temperature, the inter-platelet β-phase formed during heat treatment in the β-phase field transformed to α platelets. This resulted in a slight reduction in the normal basal texture as shown in Table 4 which summarizes the Kearns numbers of all the experimental alloys heat treated at 800°C. The resultant α platelets had a variety of habit planes and

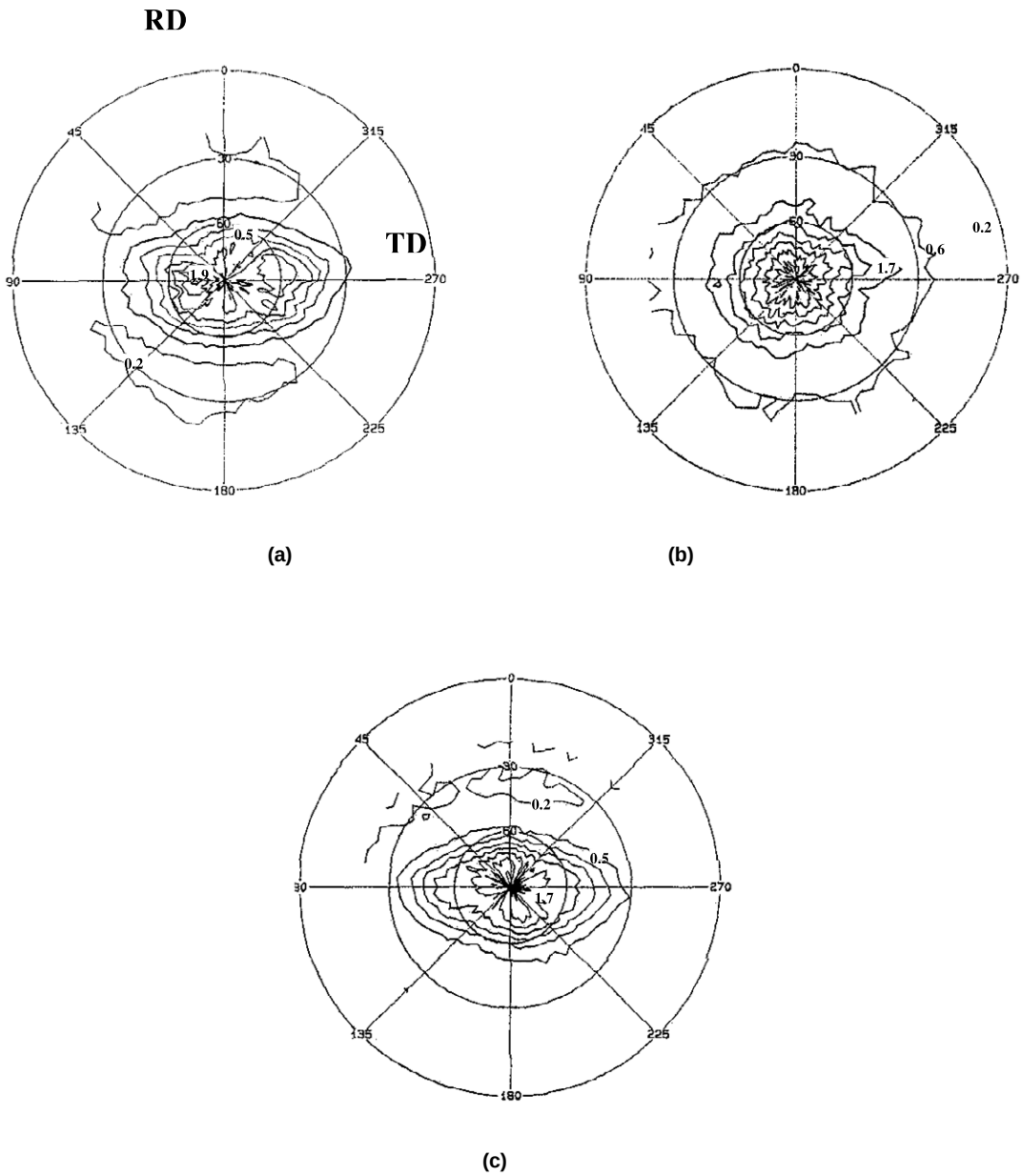

Fig. 10. Basal (0 0 0 2) pole figures of (a) Zr–1Mo, (b) Zr–1Nb and (c) Zr–1Nb–0.7Mo alloys cold-rolled 70% after β-annealing.

crystal orientations according to the Burger's orientation relationship between β- and α-phase. Fig. 8 shows a TEM image of such α-platelets transformed from the β-phase.

As stated above, the average size of equiaxed-grains varied with the alloy composition and the heat-treatment time at 800°C. A certain relationship between the grain size and the crystal texture was sought. For this purpose, the heat-treated alloys were cold-rolled again by 55% and their crystal texture was studied as a function of the grain size prior to cold rolling. As illustrated in Fig. 9, the Kearns numbers varied with the grain size and the alloy composition in a complex way. For Zr–Nb alloy systems, particularly the Zr–2.5Nb alloy, f_n increased with the grain size whereas this trend was not present in the alloys containing Mo.

Texture development of Zr-based alloys during cold rolling is expected to be weaker in the microstructure

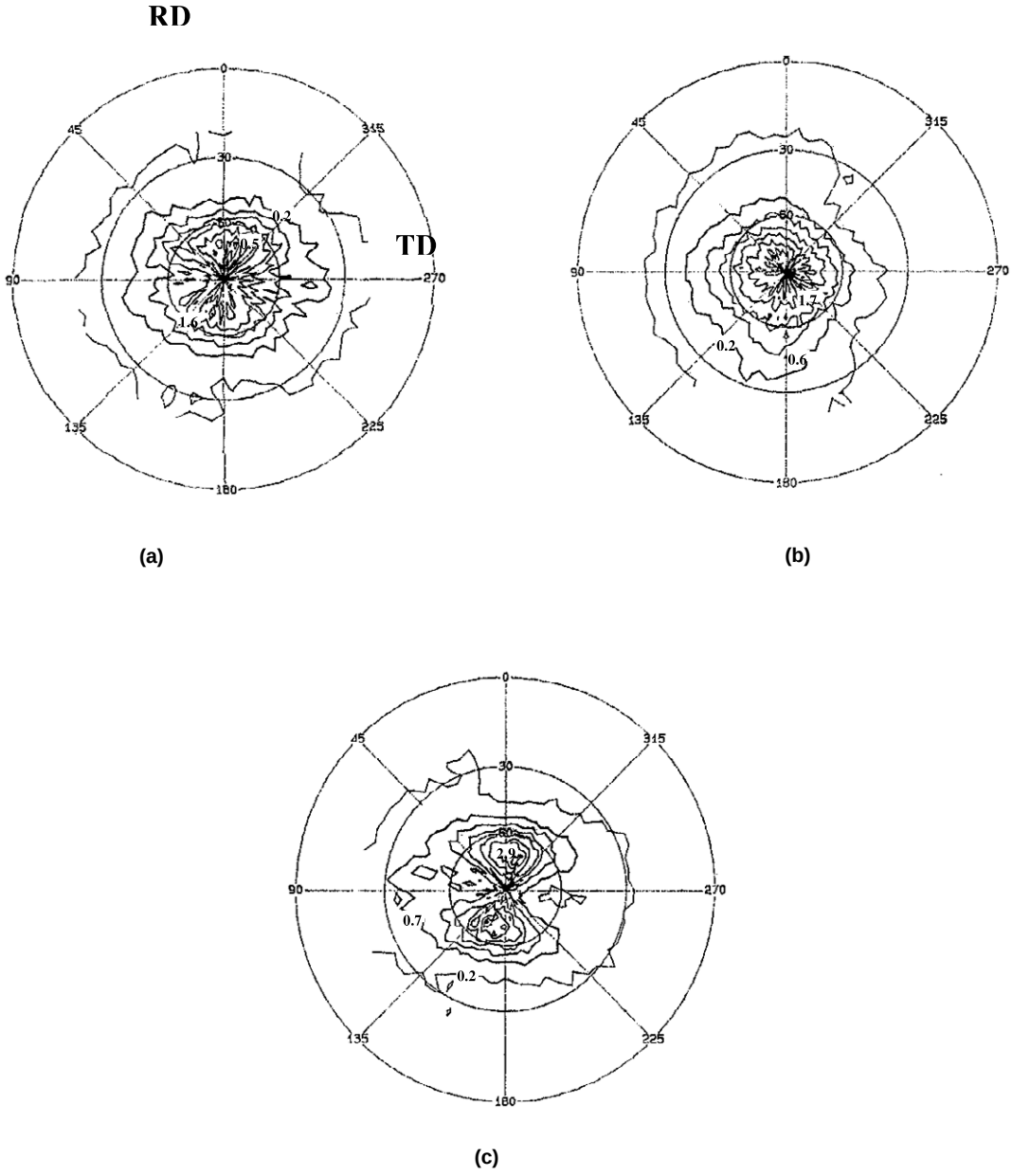

Fig. 11. Basal (0 0 0 2) pole figures of (a) Zr–1Mo, (b) Zr–1Nb and (c) Zr–1Nb–0.7Mo alloys annealed at 800°C for 350, 20 and 350 h, respectively, after the condition in Fig. 10.

consisting of smaller grains, which accounts for the trend in the Zr–Nb alloys. The effect of large grain size on diminishing the texture intensity in the Zr–Nb alloys was interpreted in terms of increased twinning propensity. The larger the grain size, the greater the number of pile-up dislocations, which in turn increased the stress build-up to generate twins [21]. In fact Doherty et al. [22,23] showed in FCC metals that the frequency of deformation twinning increased with the grain size. The apparent absence of the relationship between the texture intensity and the grain size in Mo-containing alloys is mysterious. In addition to the general reduction of texture intensity through the inherent grain-refining effect of Mo, there seems to be another mechanism operating in texture formation of the Mo-containing alloys. The texture also varied significantly with the chemical composition, especially the presence of Mo, of the experimental Zr alloys. Zr-based alloys cold-rolled for more than 50% show a bimodal basal texture that is inclined 30–40° toward

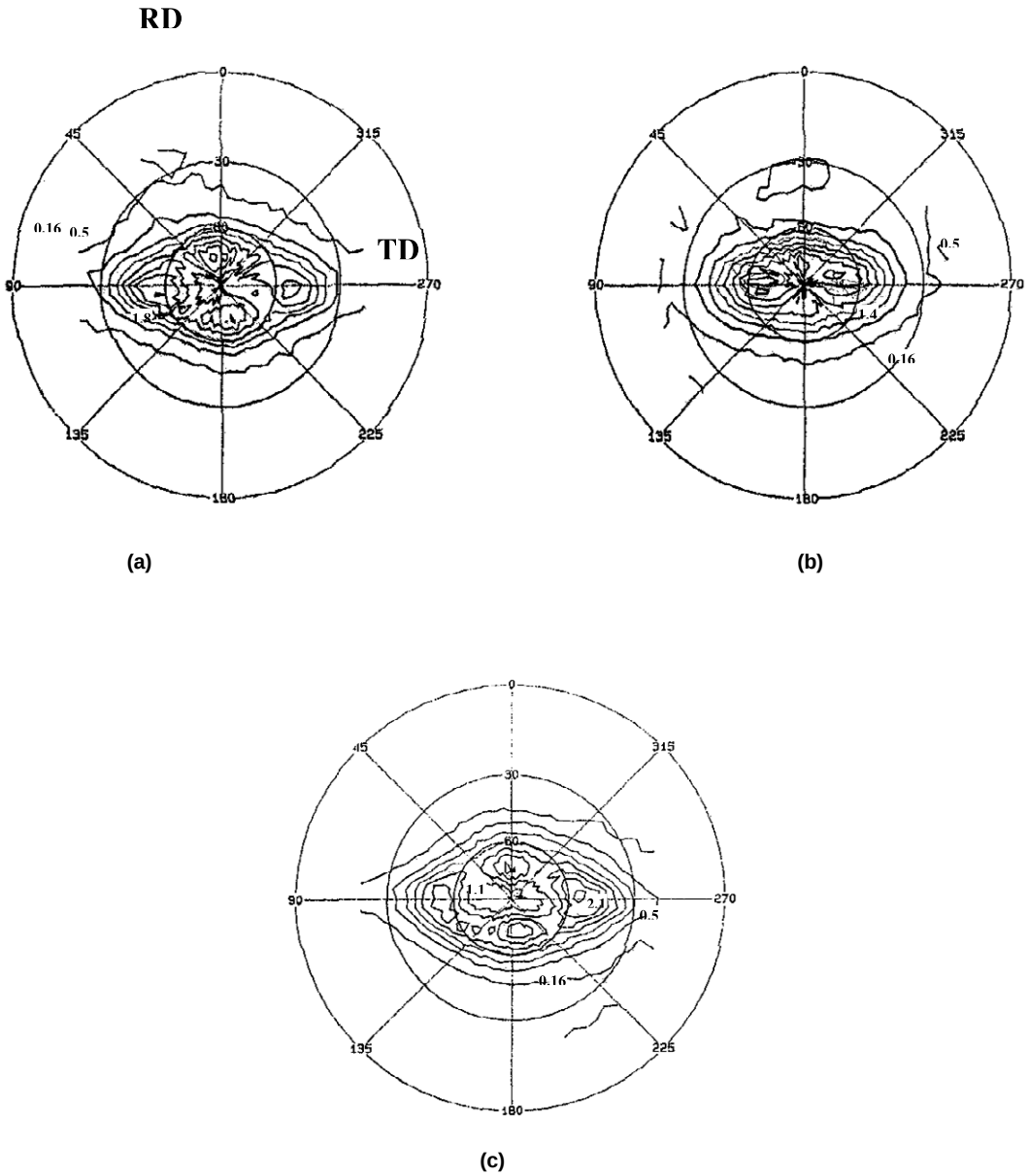

Fig. 12. Basal (0 0 0 2) pole figures of (a) Zr–1Mo, (b) Zr–1Nb and (c) Zr–1Nb–0.7Mo alloys cold-rolled 55% after the condition in Fig. 11.

TD from ND [11]. This trend was confirmed in the present experimental alloys cold worked 70% as shown in Fig. 10, although Zr–1Nb alloys showed the basal poles dispersed more evenly around ND. Since the three alloys, Zr–1Mo, Zr–1Nb and Zr–1Nb–0.7Mo had the same random texture prior to cold rolling (due to β-quenching and β-annealing) the texture difference in the cold-rolled condition was thought to be a consequence of the difference in the mode of deformation.

During annealing at 800°C the texture varied with the chemical composition of the alloys as shown in Fig. 11. In the case of Mo-containing alloys, the intensity of the basal poles changed from the even distribution along ND and TD to focused peaks at 20–30° away from ND toward RD. In contrast, Mo–free Zr–1Nb alloy showed almost no change in the texture from the cold-rolled condition. The difference in the two alloy groups was in part inherited from the prior cold-rolling condition but mostly from the relative amount of phase constituents during annealing heat treatment.

The effect of Mo on texture should be differentiated from that of grain size. For this purpose, the samples were β-annealed for various amount of time, from 20 to 350 h, and then cold-rolled. During the heat treatment the grain size was grown to about 10 μm in all the samples. Cold rolling (55%) gave these samples a common tendency of the basal pole rotation toward 30–40° ND–TD as shown in Fig. 12. Under this situation, however, the effect of Mo was clearly perceived in that the basal pole intensity was still relatively strong at the ND/RD orientation.

The effect of Mo on the texture of the experimental alloys will be discussed in terms of the mode of deformation and phase stability. As stated above, the texture varied sensitively with the processing condition and Mo content. When a random microstructure was cold-worked Mo–free Zr–1Nb alloy showed a tendency of its basal poles aligning along ND. In the case of the Mo-containing alloy, however, the tendency was suppressed by Mo addition. Weakening of the normal basal texture by Mo seems to be related to the mode of deformation as suggested by Salinas-Rodriguez [24]. It is deduced that Mo decreased the activity of twinning and promoted $c + a$ slip. The texture is also dependent on the relative stability of β-phase against $\beta \rightarrow \alpha$ transformation since it occurs according to a certain orientation relationship. Due to the stabilizing effect of Mo, the Mo-containing alloys are expected to have larger amount of β prior to transformation to α. TEM study to seek the clue was largely unsuccessful, partly due to the coarseness of the twins. A set of TEM images of a twin formed during rolling of recrystallized Zr–1Nb–0.7Mo alloy is shown in Fig. 13. Fewer twins were found in the Mo-containing alloy compared to Mo–free Zr–1Nb alloy. Except for this fact, however, no significant difference was found in the shape of twins in the two alloys. It is possible that the different roles of Nb and Mo originated from the larger atomic size misfit between Zr and Mo compared to that between Zr and Nb. More study is needed to clarify this point explicitly.

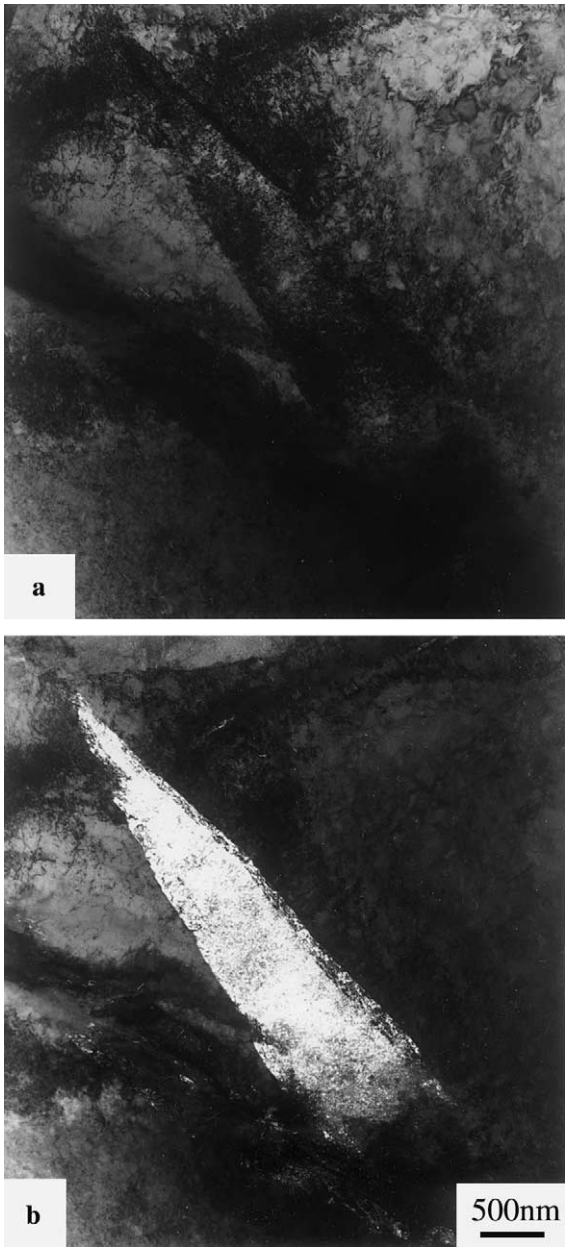

Fig. 13. TEM images of a twin in Zr–1Nb–0.7Mo alloy annealed at 800°C for 350 h and cold-rolled (55%): (a) bright field image and (b) dark field image. The twins in the Mo-containing alloy were scanty and their growth was less active than that of Mo-free counterpart.

4. Conclusions

The following conclusions were made from the study of the effect of Mo on crystal texture and twinning in Zr–Nb alloy:

1. Molybdenum addition results in a general grain refinement in Zr–Nb alloys of either beta heat-treated condition as well as alpha recrystallization heat-treated condition. Molybdenum also reduces twinning tendency of the Zr-based alloys during the early stage of cold working. The two effects combine to reduce the normal basal texture of Zr–Nb plates.
2. In Zr–Nb as well as in Zr–Nb–Mo alloys, the boundaries of α-platelet packets effectively blocked propagation of twins, limiting the length of them. Therefore the refinement of the packet size by Mo was responsible for the decreased areal density of twins.
3. In the absence of Mo, a Zr–1Nb alloy showed an increasing frequency of deformation twinning with grain size, which led to a strong normal basal texture in the alloys of coarse grain structure. Promotion of twinning in large grains was attributed to increased dislocation pile-ups and consequent stress build-up against grain boundaries.
4. The effect of Mo on the texture of the Zr alloys could be summarized as weakening the normal basal texture and promoting a texture shift during annealing heat treatment. These effects were attributed to the reduced tendency of twinning and stabilization of β-phase, respectively, by Mo-addition.

Acknowledgements

This work was supported by Korea Institute of Science & Technology Evaluation and Planning under 1999 Basic Research Program in Atomic Energy Technology. The authors are grateful to Mr J.H. Lee for his effort in editing of the manuscript.

References

[1] F. Garzarolli, H. Stehle, E. Steinberg, in: E.R. Bradley, G.P. Sabol (Eds.), Eleventh International Symposium on Zirconium in the Nuclear Industry, ASTM STP 1295, American Society for Testing of Materials, Philadelphia, PA, 1996, p. 12.
[2] D. Cubicciotti, R.L. Jones, B.C. Syrett, Stress corrosion cracking of zircaloys, EPRI Report NP-1329, Electric Power Research Institute, Palo Alto, CA, 1979.
[3] A. Tasooji, R.E. Einziger, A.K. Miller, in: D.G. Franklin, R.B. Adamson (Eds.), Sixth International Symposium on Zirconium in the Nuclear Industry, ASTM STP 824, American Society for Testing of Materials, Philadelphia, PA, 1984, p. 595.
[4] D.O. Northwood, U. Kosasih, Int. Met. Rev. 28 (1983) 92.
[5] J.H. Kim, S.K. Hwang, M.H. Kim, S.I. Kwun, Y.S. Kim, J. Kor. Inst. Met. 35 (1997) 1271.
[6] Y.B. Chun, S.K. Hwang, M.H. Kim, S.I. Kwun, Y.S. Kim, J. Nucl. Mater. 265 (1999) 28.
[7] Y.B. Chun, S.K. Hwang, M.H. Kim, S.I. Kwun, Scripta Mater. 40 (1999) 1165.
[8] J. Crépin, T. Bretheau, D. Caldemaison, Acta Metall. Mater. 43 (1995) 3709.
[9] E. Tenckhoff, in: J.H. Schemel, H.S. Rosenbaum (Eds.), Zirconium in Nuclear Applications, ASTM STP 551, American Society for Testing and Materials, Philadelphia, PA, 1974, p. 179.
[10] S.T. Mahmood, K.L. Murty, in: C.M. Eucken, A.M. Garde (Eds.), Ninth International Symposium on Zirconium in the Nuclear Industry, ASTM STP 1132, American Society for Testing of Materials, Philadelphia, PA, 1991, p. 119.
[11] E. Tenckhoff, Metall. Trans. 9A (1978) 1401.
[12] R.G. Ballinger, G.E. Lucas, R.M. Pelloux, J. Nucl. Mater. 126 (1984) 53.
[13] J.J. Kearns, Thermal expansion and preferred orientation in zircaloy, Westinghouse Elec. Co. Report, WAPD TM-472, 1965.
[14] A.V. Chirkin, A.S. Al-Nakow, S.M. Sherif, J. Nucl. Mater. 178 (1991) 27.
[15] Salinas Rodriguez, Acta Metall. Mater. 43 (1995) 485.
[16] E. Tenckhoff, in: D.G. Franklin (Ed.), Fifth Conference on Zirconium in the Nuclear Industry, ASTM STP 754, American Society for Testing of Materials, Philadelphia, PA, 1982, p. 5.
[17] U.F. Kocks, C.N. Tomé, H.-R. Wenk, in: Texture and Anisotropy, Cambridge University, UK, 1998.
[18] W.G. Burgers, Physica 1 (1934) 561.
[19] R.W. Hertzberg, in: Deformation and Fracture Mechanics of Engineering Materials, Wiley, New York, 1996.
[20] F.J. Humpherys, M. Hartherly, in: Recrystallization and Related Annealing Phenomena, Pergamon, UK, 1996.
[21] S. Mahajan, D.F. Williams, Int. Metall. Rev. 18 (1973) 43.
[22] S. Asgari, E. El-Danaf, S.R. Kalidindi, R.D. Doherty, Metall. Trans. 28A (1997) 1781.
[23] E. El-Danaf, S.R. Kalidindi, R.D. Doherty, Metall. Trans. 30A (1999) 1223.
[24] A. Salinas-Rodriguez, M.G. Akben, J.J. Jonas, E.F. Ibrahim, Can. Quart. 24 (1985) 259.